ACS NANO
Cite This: ACS Nano XXXX, XXX, XXX–XXX
www.acsnano.org

ARTICLE

Nanocrystals in Molten Salts and Ionic Liquids: Experimental Observation of Ionic Correlations Extending beyond the Debye Length

Vladislav Kamysbayev,[†,∥] Vishwas Srivastava,[†,∥] Nicholas B. Ludwig,[†,∥] Olaf J. Borkiewicz,[‡] Hao Zhang,[†] Jan Ilavsky,[‡] Byeongdu Lee,[‡] Karena W. Chapman,[‡,⊥] Suriyanarayanan Vaikuntanathan,[†] and Dmitri V. Talapin*[,†,§]

[†]Department of Chemistry and James Franck Institute, University of Chicago, Chicago, Illinois 60637, United States
[‡]X-ray Science Division, Advanced Photon Source, Argonne National Laboratory, Argonne, Illinois 60439, United States
[§]Center for Nanoscale Materials, Argonne National Laboratory, Argonne, Illinois 60439, United States

Supporting Information

ABSTRACT: The nature of the interface between the solute and the solvent in a colloidal solution has attracted attention for a long time. For example, the surface of colloidal nanocrystals (NCs) is specially designed to impart colloidal stability in a variety of polar and nonpolar solvents. This work focuses on a special type of colloids where the solvent is a molten inorganic salt or organic ionic liquid. The stability of such colloids is hard to rationalize because solvents with high density of mobile charges efficiently screen the electrostatic double-layer repulsion, and purely ionic molten salts represent an extreme case where the Debye length is only ~1 Å. We present a detailed investigation of NC dispersions in molten salts and ionic liquids using small-angle X-ray scattering (SAXS), atomic pair distribution function (PDF) analysis and molecular dynamics (MD) simulations. Our SAXS analysis confirms that a wide variety of NCs (Pt, CdSe/CdS, InP, InAs, ZrO_2) can be uniformly dispersed in molten salts like $AlCl_3$/NaCl/KCl ($AlCl_3/AlCl_4^-$) and NaSCN/KSCN and in ionic liquids like 1-butyl-3-methylimidazolium halides ($BMIM^+X^-$, where X = Cl, Br, I). By using a combination of PDF analysis and molecular modeling, we demonstrate that the NC surface induces a solvent restructuring with electrostatic correlations extending an order of magnitude beyond the Debye screening length. These strong oscillatory ion−ion correlations, which are not accounted by the traditional mechanisms of steric and electrostatic stabilization of colloids, offer additional insight into solvent−solute interactions and enable apparently "impossible" colloidal stabilization in highly ionized media.

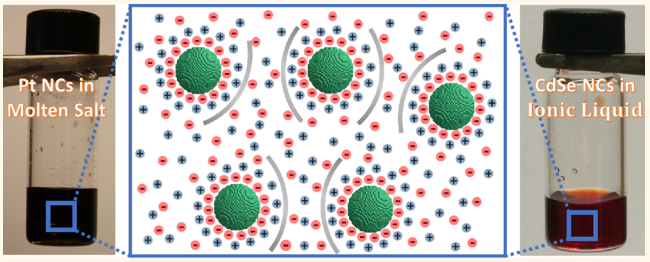

KEYWORDS: *solvent restructuring, colloidal nanocrystals, molten salts, ionic liquids, small-angle X-ray scattering, X-ray pair distribution function, molecular dynamics simulations*

The colloidal state is realized by preventing irreversible aggregation of solute particles dispersed in a solvent. A "good" solvent inhibits the aggregation and disperses particles forming a stable colloidal solution. Traditionally, long chain hydrocarbons with a surface-binding headgroup have been employed as ligands to disperse nanocrystals (NCs) in nonpolar organic solvents.[1] The basis for this type of stabilization (steric) is the minimization of the free energy associated with the chain-solvent mixing,[2] which is accomplished by the repulsion of hydrocarbon chains tethered to the surface of NCs.[3] A fundamentally different way to provide colloidal stability to NCs is through electrostatic effects, where charged groups are adsorbed on the NCs' surface and their charge is balanced by a diffuse cloud of counterions.[3] In this case, a good solvent is one with a high dielectric constant that can effectively screen the electrostatic attraction between oppositely charged surface-bound and dispersed ions.[2] Combined together, these two mechanisms complement each other in providing colloidal stability to NCs in a wide variety of solvents.

Received: February 15, 2019
Accepted: April 8, 2019
Published: April 9, 2019

DOI: 10.1021/acsnano.9b01292
ACS Nano XXXX, XXX, XXX–XXX

Apart from providing colloidal stability to NCs, solvents also play a critical role in governing the nucleation and growth dynamics during NC synthesis.[4,5] A wide variety of nanomaterials such as semiconductor quantum dots,[6] oxide[7] and metal[8] nanoparticles can be synthesized in a precise manner in either organic or aqueous media. However, our ability to synthesize many hard-to-crystallize inorganic phases in a nanocrystalline form is limited by the inability of currently available solvents to reach desired crystallization temperatures.[9,10] Very few traditional solvents remain liquid and stable above 400 °C, but many inorganic phases require even higher temperatures to form and anneal out structural defects.[9] The exploration of unconventional solvent systems and understanding their interaction with the NC surface is therefore essential for synthetic development of next-generation inorganic nanomaterials.

Our group recently reported on the formation of colloidal solutions of NCs dispersed in molten inorganic salts.[11] Molten inorganic salts represent a very attractive class of solvents for the synthesis and processing of nanomaterials due to their high temperature stability, wide electrochemical window, stability in the presence of highly reactive species, the ability to dissolve many ionic solids not soluble in traditional solvents, and transparency in a broad range of the electromagnetic spectrum.[11,12] Molten inorganic salts have long been used as inert or reactive fluxes for solid-state chemistry,[13] crystal growth,[14,15] and electrolysis of refractory metals.[16,17] Molten salt fluxes have been explored for the synthesis of nanostructured oxides, metal alloy NCs,[18] and covalent compounds (metal boride,[19] SiC,[20] Si,[21,22] graphene,[23] and carbon nanotubes[24]). Colloidal stability is a critical requirement for precise synthesis and chemical manipulations of nanomaterials at high temperatures. As we have shown in previous studies, the ability to engineer interactions between the NC surface and the molten inorganic salt helps when performing precise chemical manipulations on the NCs, such as defect annealing and cation exchanges, while preserving their shape and size homogeneity.[9,25]

The stability of NCs in molten inorganic solvents has to be explained by a mechanism fundamentally different from traditional steric and electrostatic approaches. A very high charge density of molten salt results in a Debye screening length $L_D = 1/\sqrt{4\pi\rho q^2/\varepsilon k_B T}$ (where ρ is the ion concentration per unit volume, q is the unit charge, ε is the dielectric constant, and $k_B T$ is the thermal energy), which is only ∼1 Å. Such extremely short-ranged screening makes electrostatic stabilization in the classical sense impossible, while the absence of long chain ligands on the NC surfaces eliminates the possibility of steric stabilization. Empirically, we found that only specific salts with pronounced chemical affinity for the nanoparticle's surface were able to impart colloidal stability.[11] It was observed that molten salts with ions which were able to function as X- or Z-type ligands to the nanoparticle surface were able to stabilize them. Both halides and SCN^- are examples of X-type ligands (Lewis basic) whereas $AlCl_3$ belongs to the category of Z-type ligands (Lewis acidic).

Organic ionic liquids (ILs), a cousin of molten inorganic salts, were also found to provide colloidal stability to a variety of inorganic NCs. ILs with pronounced Lewis basicity but limited steric bulk, such as those belonging to the class of $BMIM^+X^-$, formed stable dispersions of CdSe NCs where X^- = Cl^-, Br^-, I^-, but did not support any colloidal stability when X^- = BF_4^- (Lewis Neutral).

Based on the recent direct force−distance measurements using Surface Force Apparatus, interactions between charged surfaces in aprotic organic ILs consist of the short-range oscillatory and long-range electrostatic components.[26,27] While the origin of the long-range repulsion is a subject of active experimental and theoretical studies,[28−30] the short-range oscillatory interaction is believed to be due to the ion layering near the surfaces. Experimentally, such structural changes of ionic solvents next to flat surfaces have been verified by X-ray reflectivity,[31] angle-resolved X-ray photoelectron spectroscopy (XPS),[32] and sum-frequency generation spectroscopy.[33] However, these surface sensitive techniques are not suitable for studying colloidal solutions. Recently X-ray pair distribution function (PDF) analysis has been successfully applied to study reorganization of molecular solvents around colloidal particles[34,35] and ILs confined inside carbon nanopores.[36]

Here, we report an experimental observation of enhanced layering of ions in the molten salt around colloidal NCs revealed by the PDF analysis of total X-ray scattering data. Such restructuring of the solvent is templated by the layer of surface-bound ions and responsible for the formation of noninteracting colloids or, in some cases, weakly aggregated structures that do not precipitate, as evidenced by SAXS measurements. We believe this work will advance our understanding of the intermediate range ion correlations in highly ionized media. Through this work, we also aim to establish molten salts as versatile solvents for nanomaterials synthesis and processing, especially at temperatures beyond the reach of more traditional solvents.[9,25]

RESULTS AND DISCUSSION

An inorganic molten salt or IL with a pronounced Lewis acidic or Lewis basic character can be used to colloidally stabilize NCs of metals (Pt), oxides (ZrO_2), and binary semiconductors (CdSe, InP, InAs). We chose molten eutectics of $AlCl_3$/NaCl/KCl ($AlCl_3/AlCl_4^-$) and NaSCN/KSCN as representatives of salts with Lewis acidic and Lewis basic character, respectively. We also studied NC dispersions in $BMIM^+X^-$ (where X = Cl, Br, I) ILs which represent the organic analog of inorganic molten salts. In the case of NaSCN/KSCN molten salt, NCs were first stripped of their original organic ligands and the dried NC powders were stirred in the molten salt for several hours until a uniform dispersion was formed. In the case of $AlCl_3/AlCl_4^-$ molten salt and $BMIM^+X^-$ ILs, NCs could phase transfer directly from the organic phase after interfacing it with the respective ionic media. A concentration of ∼1 mg/mL NCs in molten salts and ILs was used for all experiments, unless specified otherwise. A complete list of NCs and molten salt combinations explored in this work is provided in Table S1. Representative photographs of NC dispersions in ionic solvents are shown in Figure 1a. The NCs retained their morphology as evidenced by transmission electron microscopy (TEM) images taken before and after their dispersion in the molten salt (Figures 1b, c). Our choice of solvents was motivated by the following: (i) low melting points (97 °C for $AlCl_3/AlCl_4^-$, 140 °C for NaSCN/KSCN, and ∼73 °C for $BMIM^+Cl^-$) for easy handling; (ii) sufficient transmission of X-rays for both small-angle X-ray scattering (SAXS) and total X-ray scattering experiments; and (iii) chemical affinity of the molten salt to NC surfaces, as previously reported for halide, halometallate, and SCN^- ions.[37−39]

DOI: 10.1021/acsnano.9b01292
ACS Nano XXXX, XXX, XXX−XXX

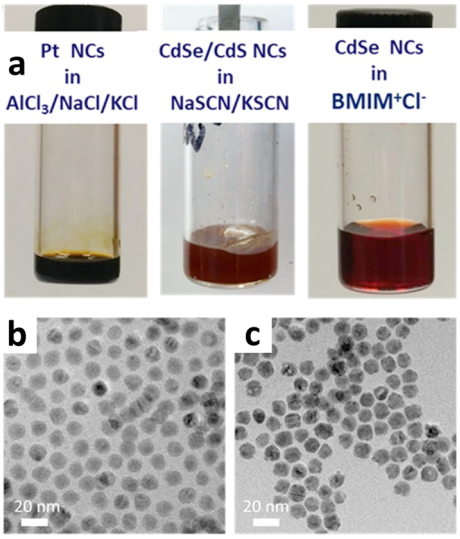

Figure 1. (a) Representative photographs of NC colloids in molten salts and ionic liquids. (b,c) TEM images of CdSe/CdS NCs (b) before dispersing in molten NaSCN/KSCN eutectic and (c) after their recovery from NaSCN/KSCN eutectic and functionalization with organic ligands.

A representative SAXS curve of Pt NCs in molten $AlCl_3/AlCl_4^-$ is shown in Figure 2a. The SAXS curve for the same Pt NCs in toluene is shown for comparison. In the case of SAXS from NCs, it is common to assume that the scattering intensity, $I(q)$, is a product of two terms (decoupling approximation), the form factor, $F(q)$, which defines particle shape and size polydispersity, and the structure factor, $S(q)$, which carries the information about organization and interactions between NCs: $I(q) = |F(q)|^2 S(q)$.[40] The fitting of the experimental data yielded $S(q) \sim 1$ for Pt NCs in molten $AlCl_3/AlCl_4^-$ (Figure S1), meaning that the scattering is determined by the form factor only (dilute limit) and particles do not interact with each other, much like they behave in toluene. The volume size distributions extracted for the two curves using the form factors of a sphere nearly overlap suggesting that there was no ripening of Pt NCs in molten salt (Figure S2).

Dispersions of NCs in NaSCN/KSCN eutectic show qualitatively similar behavior, forming nonprecipitating colloidal solutions in the melt. However, SAXS measurements show that NCs in NaSCN/KSCN melt do not form a noninteracting (dilute limit) colloid but rather a loose network of particles, here shown for the dispersions of CdSe/CdS core–shell NCs in NaSCN/KSCN melt. CdSe/CdS core–shells were chosen for these experiments due to (i) tight size distribution; (ii)

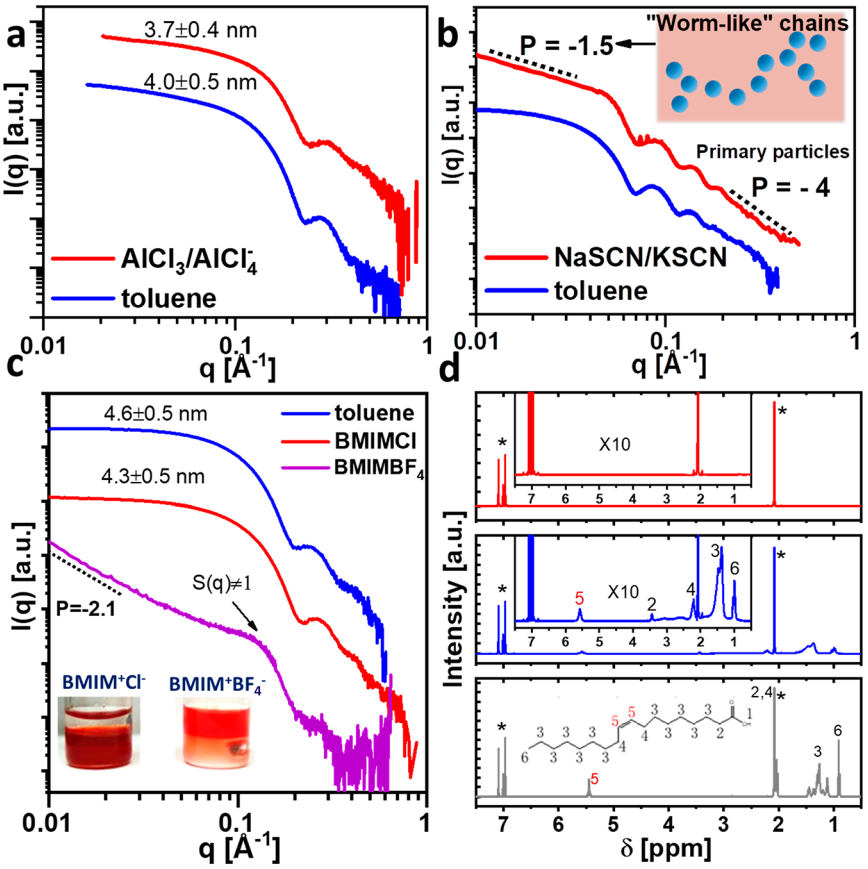

Figure 2. Characterization of NCs dispersed in different salts and comparison to the same NCs in toluene: (a) SAXS curves for Pt NCs dispersed in molten $AlCl_3/AlCl_4^-$ eutectic (red) and the same NCs dispersed in toluene (blue). (b) SAXS curves for CdSe/CdS core–shells in molten NaSCN/KSCN eutectic (red) and the same NCs dispersed in toluene (blue). (c) SAXS curves of CdSe NCs in $BMIM^+X^-$ ILs and toluene (Note: In the case of $BMIM^+BF_4^-$ solution, the Porod region of CdSe NCs with the intensity decaying as q^{-4} is obscured due to the interference from the WAXS of $BMIM^+BF_4^-$). The inset shows a successful transfer of CdSe NCs from the top nonpolar phase to Lewis basic $BMIM^+Cl^-$ IL and no transfer in the case of Lewis neutral $BMIM^+BF_4^-$ IL. (d) ^1H NMR spectra of oleic acid (gray curve), CdSe NCs capped with oleic acid in d^8-toluene (blue curve) with the assignments of resonances in the inset and diethyl ether extract of digested CdSe NCs recovered from $BMIM^+Cl^-$ (red curve) (asterisk (*) indicates residual solvent resonances).

DOI: 10.1021/acsnano.9b01292
ACS Nano XXXX, XXX, XXX–XXX

good stability at temperatures above 200 °C; and (iii) affinity of the NC surface to SCN^- ions. Figure 2b shows a representative SAXS curve of core−shell NCs stripped of the original organic ligands (further referred to as "bare NCs") and dispersed in NaSCN/KSCN molten salt. In this case the NCs interacted with each other resulting in a nonconstant $S(q)$ across the measured q range (Figure S3). The slope of −1.5 observed for the $I(q)$ curve at $q < 4 \times 10^{-2}$ Å^{-1} suggests that the NCs form mass fractal-like aggregates whose dimension can be inferred from the power law slope.[41] A low q slope of −1.5 corresponds to the fractal dimension of 1.5.[42] Fractal dimensions below 2 suggest formation of the open "wormlike" secondary structures. The reversible formation of chain structures has been previously reported for charged particles.[43,44] $I(q)$ for $q > 4 \times 10^{-2}$ Å^{-1} (Figure 2b) shows the Bessel function oscillations with the Porod slope of −4, same as for CdSe/CdS NCs of similar size dispersed in toluene suggesting the preservation of the spherical shape and size distribution of NCs in the melt (Table S2). For the NCs dispersed in the NaSCN/KSCN melt, the average separation between individual particles can be assessed by Fourier transforming the structure factor $S(q)$ resulting in the pair distribution function, PDF-SAS.[45] To understand the role of the molten salt in preserving particle separation, we compared PDF-SAS of bare CdSe/CdS NCs dispersed in molten NaSCN/KSCN eutectic at 250 °C with that of an annealed film of bare NCs (Figure S4). The average interparticle distance is ∼5 Å for NCs in NaSCN/KSCN melt whereas it changed from ∼3 Å for same NCs aggregated in-film at room temperature to ∼0 Å (Table S2) after annealing the film at 250 °C. The average interparticle distance of 5 Å suggests on average ∼5/3.3 = 1.5 ion pairs of K^+-SCN^- where 3.3 Å is the size of K^+-SCN^- ion-pair derived from the atomic PDF analysis detailed later in this report (Figure S13a).[46] An approximate, phenomenological theory predicts a secondary free energy minimum when CdSe/CdS NCs are ∼ 5 Å apart (Figure S5). Here the NCs have to surmount a potential barrier of at least an order of magnitude greater than k_BT before they can contact directly. Moreover, CdSe/CdS NCs dispersed in NaSCN/KSCN melt and heated to 250 °C could be recovered and redispersed in a nonpolar solvent such as hexane with the help of organic ligands, while the same NCs annealed at the same temperature without molten salts could not be redispersed into a solution. TEM images of these NCs showed a clear evidence of necking while no necking was observed for the CdSe/CdS core−shells recovered from the molten NaSCN/KSCN eutectic (Figure S6).

In addition to molten inorganic salts, SAXS measurements were carried out on NC dispersions in $BMIM^+X^-$ ILs. Similar to molten inorganic salts, $BMIM^+X^-$ ILs are unlikely to provide steric or electrostatic stabilization to NC colloids. However, CdSe NCs form stable noninteracting colloids in halide containing $BMIM^+X^-$ (X = Cl, Br, I) ILs. SAXS curves of CdSe NCs in these ILs show $I(q)$ approaching $S(q)$ (Figure S7) in the Guinier region at $q < 1/R_g$, where R_g is the radius of gyration, 1.7 nm for CdSe NCs, suggesting absence of NC aggregates (Figure 2c). We further confirmed the absence of organic ligands on CdSe NCs recovered from their IL dispersions by carrying out ^{1}H NMR measurements and comparing them to CdSe NCs capped with oleic acid ligands (see the Supporting Information for experimental details). Characteristic resonances corresponding to the oleic acid ligands were completely absent in the ^{1}H NMR spectrum of NCs recovered from $BMIM^+Cl^-$ IL (Figure 2d). Additionally, the FTIR spectrum of the recovered CdSe NCs resembles that of the pure $BMIM^+Cl^-$ IL (Figure S8), thus suggesting complete removal of the native ligands during the phase transfer and ruling out steric mode of stabilization. Further, we observed a universal ∼0.3 nm decrease of the average size of CdSe NCs in $BMIM^+X^-$ ILs from the fitting of SAXS curves, which can be attributed to the removal of bound $Cd(oleate)_2$ from the CdSe NC surface. Although $BMIM^+BF_4^-$ IL could not directly transfer CdSe NCs from the nonpolar phase (Figure 2c, inset), CdSe NCs could first be stripped of their native oleic acid and suspended in this Lewis neutral IL which does not contain ions capable of strongly binding to NC surface. In contrast to halide containing ILs, organic-ligand-free CdSe NCs in $BMIM^+BF_4^-$ IL exhibited a rising low q intensity with the power law slope of −2.1 indicating that they failed to form a stable colloidal solution (Figure 2c, purple curve, and Figure S9). This observation demonstrates that absence of the native organic ligands alone is not sufficient to render particles stable in ionic media but a strong chemical affinity of the solvent ions to the NC surface is required to impart colloidal stability. InAs NCs could also form stable colloidal solutions in halide containing ILs demonstrating the generality of this interaction. Similar to the dispersion of CdSe NCs, the SAXS intensity levels off at $q < 1/R_g$ (Guinier region) and exhibits $S(q) \sim 1$ (Figure S10).

Next, we sought to characterize the chemical nature of the interaction between the salts and the NCs in more detail. The vibrational fingerprint of the SCN^- ion was used as an indicator for the nature of chemical bonding of SCN^- ions and the NC surface in molten inorganic salts.[39] We measured FTIR spectra of NCs recovered from molten NaSCN/KSCN eutectic and compared them to free SCN^- ions (Figure 3a). Free SCN^- ion shows a distinct IR absorption band corresponding to the CN stretch near 2060 cm^{-1} while CdSe/CdS NCs recovered from the molten NaSCN/KSCN showed this feature shifted to 2090 cm^{-1}. This positive shift in the CN stretching frequency can be attributed to the binding of the SCN^- ion to the surface Cd atoms through the sulfur atom. A larger shift to 2110 cm^{-1} was observed for SCN^- ions bound to Pt NCs suggesting stronger C≡N bond due to greater π-back bonding of Pt 5d-electrons to the π^* molecular orbitals of SCN^- ions.

Similar evidence of chemical bonding could also be observed for NCs dispersed in ILs, using XPS. For these measurements, we used InAs NCs dispersed in $BMIM^+I^-$ as our sample of choice due to the substantial difference in the binding energy of In−I and In−As bonds, and the ability to distinguish In−I bonds from possible In−O bonds which could form during sample preparation. We compared the In 3d high resolution XPS spectrum of tri-*n*-octyl phosphine capped InAs NCs with that of InAs NCs recovered from $BMIM^+I^-$ IL. InAs NCs recovered from $BMIM^+I^-$ showed a distinct contribution from In−I bonds whose peak is shifted by 1.1 eV (In $3d_{5/2}$ at 445.1 eV), indicating a higher effective oxidation state of In bound to I than In bound to As (Figure 3b).[47] For reference, the In $3d_{5/2}$ XPS signal of In_2O_3 is expected at 443.8 eV and that of InO(OH) is expected at 444.3 eV.[48] These results unequivocally prove that highly specific chemical interactions exist between the NC surface and Lewis basic ions in both the molten inorganic salts and organic ILs, which may be critical for understanding the colloidal stabilization in these media.

DOI: 10.1021/acsnano.9b01292
ACS Nano XXXX, XXX, XXX−XXX

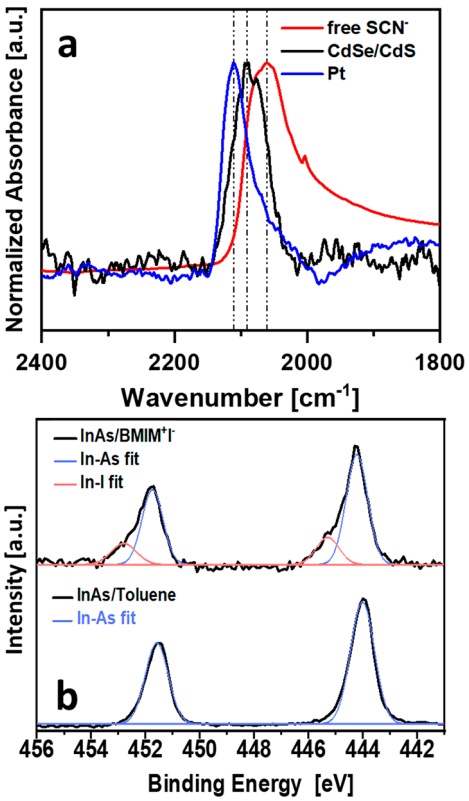

Figure 3. (a) FTIR spectra of Pt, CdSe/CdS NCs recovered from NaSCN/KSCN melt in comparison with pure NaSCN/KSCN salt. (b) High resolution XPS spectra of In 3d core region for the original InAs NCs and InAs NCs recovered from $BMIM^+I^-$ IL.

Any changes in local structure of molten inorganic salts and ILs induced by the addition of NC solute can be probed directly with the atomic PDF analysis of the high energy X-ray scattering patterns. PDFs are extracted by the Fourier transform of the total X-ray scattering data and can give information about both short-range order (arrangement of atoms within molecules, sharp peaks at 1−5 Å) and intermediate-range order (intermolecular arrangements, broad oscillations at 3−20 Å) in a liquid sample. This ability to probe intermediate-range order can give us valuable information about the solvent layer immediately next to the NC surface. The compositional diversity in the $AlCl_3/AlCl_4^-$ eutectic due to the high vapor pressure of $AlCl_3$ and the presence of small amounts of $Al_2Cl_7^-$ and $Al_3Cl_{10}^-$ ions presented a hurdle for the interpretation of PDF data in these salts.[49] Therefore, we focused our attention primarily on the NaSCN/KSCN eutectic and $BMIM^+X^-$ ILs. We obtained scattering data for the pure molten salt, NC powders without any solvent and, finally, for the NC/salt dispersions. To extract information about the structure of solvent proximal to the NC surface (restructured melt), we first subtracted the total scattering of the pure melt from the NC/salt dispersions (Figure S11) before the Fourier transform. The difference curve was further normalized by the atomic form factors of the elements in the melt rendering the reduced structure factor, RSF = $q[S(q) - 1]$, which contains element-independent structural information (Figure S12). The Fourier transform of the RSF gives us the differential-PDF (d-PDF). Further subtraction of the contribution from the NC powders results in a double-differential PDF (dd-PDF). The amplitude of oscillations (if any) in dd-PDF varied for different NCs and was found to be dependent on the concentration of NCs in the melt. We found that dilute samples (∼1 mg/mL) tended to give most pronounced oscillations. This can be attributed to two factors (1) dilute samples allowed a more precise subtraction of the contribution from crystalline nanoparticles that have higher scattering coefficients as compared to the amorphous salt matrix and (2) an ∼1 mg/mL concentration for an ∼4 nm Pt particle corresponds to an interparticle distance of ∼86 nm in a colloidal solution which is sufficiently large to negate any interference between the restructured solvent shells around NCs.

Using this PDF analysis, we see a change in the structure of the NaSCN/KSCN melt when Pt NCs are present. Any features in the d-PDF apart from the interatomic distances inside Pt NCs must be due to restructuring of the solvent induced by the presence of NCs.[34] Indeed, we observed that the d-PDF of NCs in NaSCN/KSCN melt contains peaks from the interatomic distances within Pt NCs (Figure 4a,i) superimposed over damped sinusoidal oscillations of the intermediate range order (Figure 4a,ii). In the RSF corresponding to this d-PDF, we observed the appearance of a first sharp diffraction peak (FSDP) which is distinct from that of the bulk liquid, with a shift of -0.31 $Å^{-1}$ relative to the bulk (Figure S12), and which does not appear in the Pt NC powder. After subtracting contribution of Pt NCs (Figure 4a,iii), the resultant dd-PDF contains broad oscillations corresponding to the restructured melt. In order to fit the intermediate range order with an exponentially damped sinusoidal function, the wavelength of the oscillation for the bulk and restructured NaSCN/KSCN melts was fixed at 3.3 Å which corresponds to the reported distance between K^+ and SCN^- ions in KSCN melt (Figure S13a).[46] In a highly ionic environment, the wavelength of the intermediate range order represents the physical size of the ion pair.[50] The contribution of the Na^+-SCN^- distance to the intermediate range order oscillations in NaSCN/KSCN eutectic mixture is insignificant due to (i) lower molar concentration (26.3 mol %) of the NaSCN component; and (ii) smaller X-ray scattering cross-section of Na^+ compared to that of K^+ (Figure S13b). The dd-PDF of Pt NCs in the NaSCN/KSCN melt shows oscillations with a distinct phase, amplitude, and decay length relative to the original NaSCN/KSCN melt (Figure 4b). A sharp peak at ∼2.9 Å in the dd-PDF plot for Pt NCs in NaSCN/KSCN melt likely corresponds to the distance between surface Pt atoms and S atoms of the chemisorbed sulfide and SCN^- ions forming a dense layer on Pt surface (Figure S13c). The phase change of the oscillatory component is primarily responsible for the observed shift in the FSDP of the restructured melt to smaller q position compared to that of the bulk melt (Figure S14a). As we show further for NCs in $BMIM^+Cl^-$ IL, this change in phase reflects correlations between ions in the melt and NC surface not present otherwise. An increase in the amplitude suggests higher local density of K^+/Na^+ and SCN^- ions near the Pt NC surface than in the bulk. The difference in the decay length can be more clearly visualized from a logarithmic plot of the absolute value of $G(r)$ (Figure 4c). The $1/e$ decay length increases from 3.9 Å in the bulk to 7.5 Å near the Pt NC surface suggesting that the ion−ion correlations near the Pt surface are more persistent than the ion−ion correlations in the bulk melt. This increase in the decay length is correlated with the observed increase in intensity and decrease in full width at half of the maximum of the FSDP of

DOI: 10.1021/acsnano.9b01292
ACS Nano XXXX, XXX, XXX−XXX

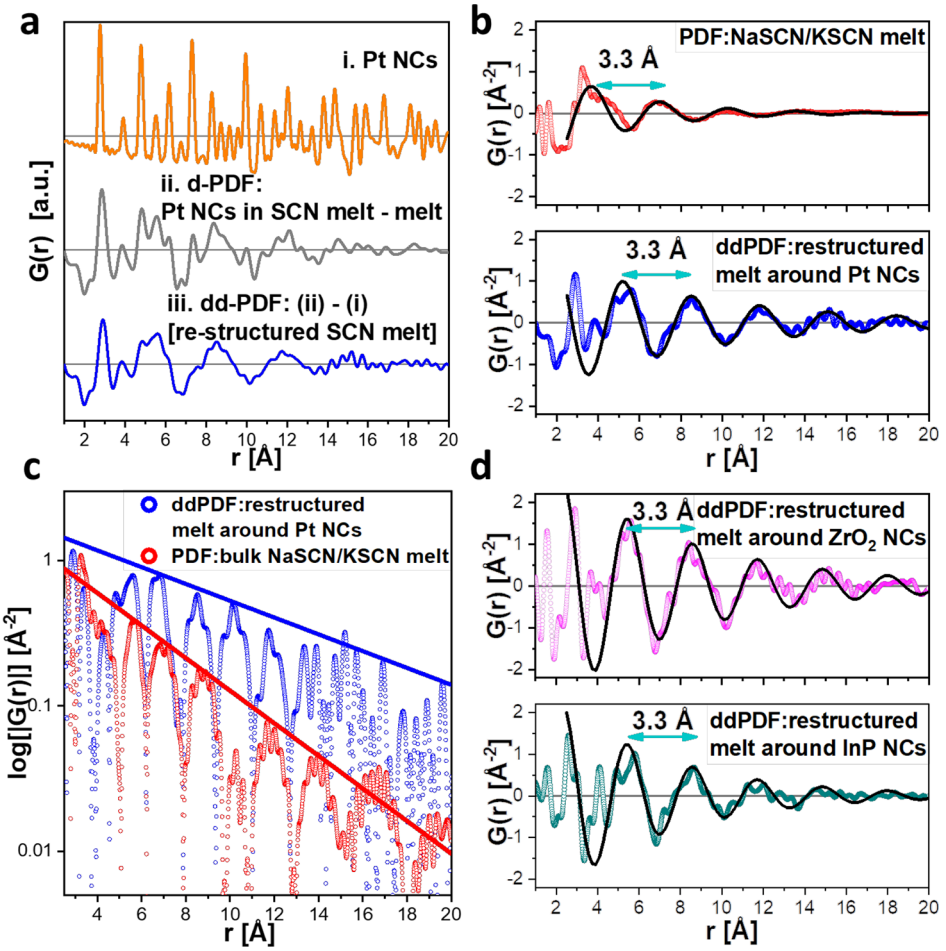

Figure 4. (a) Experimental PDF of Pt NCs in the dry powder, d-PDF of Pt NCs capped with S^{2-} ligands in NaSCN/KSCN after the bulk liquid PDF subtraction, and dd-PDF after additional subtraction of the NC contribution. (b) dd-PDF of Pt NCs and NaSCN/KSCN melt curves fitted using the exponentially damped sinusoidal functions (black curves). (c) Logarithmic plot of the curves from panel (b) showing the difference in the decay lengths between the restructured and bulk melts. (d) Comparison of the dd-PDFs corresponding to the restructured NaSCN/KSCN melt around ZrO_2 and InP NCs (black curves represent the fits).

the restructured solvent compared to that of the bulk melt (Figure S14b). We observed a similar shift in FSDP (Figure S15) and phase as well as enhancement of the amplitude and decay length for other NCs, specifically the ZrO_2 and InP NCs in NaSCN/KSCN melt (Figures 4d), showing the generality of this picture for all classes of NCs. In a control experiment using toluene as the noninteracting solvent, we observed featureless dd-PDF (Figure S16), suggesting absence of toluene restructuring around InP NCs.

We performed a similar PDF analysis for Pt NCs dispersed in $BMIM^+Cl^-$ IL (Figure S17). The shift of -0.24 $Å^{-1}$ in the FSDP for Pt NCs in the IL as compared to pure IL shows that $BMIM^+Cl^-$ restructures around the NCs (Figure S18). The wavelength of the oscillation is larger for $BMIM^+Cl^-$ than for NaSCN/KSCN melt (Figure 5a). This corroborates the fact that the wavelength represents the physical size of the ion pair. Compared to the case of the molten inorganic salt, the PDF of the restructured $BMIM^+Cl^-$ shows no pronounced change in the amplitude. However, as in the case of the NaSCN/KSCN melt, the decay length increases from 3.6 Å for the bulk IL to 4.4 Å for the restructured IL (Figure S19). Faster decay of the ion−ion correlations and lower ionic density (smaller oscillation amplitude) near the nanostructured surfaces can be attributed to the bulkier and less polarizable nature of $BMIM^+-Cl^-$ ion pair compared to small inorganic K^+/Na^+ and SCN^- ions. In addition to Pt NCs, CdSe and InP NCs in $BMIM^+Cl^-$ IL exhibited dd-PDFs with a distinct phase and increased decay length (Figure 5b).

MD simulations of NCs in $BMIM^+Cl^-$ further indicate that the distinct phase and decay length of the intermediate range oscillatory components in dd-PDFs originate from the correlations between the ions and NC surface. Our choice to study $BMIM^+Cl^-$ was in part motivated by the availability of the force fields for this IL, which enabled direct comparison of experimental data and MD models.[51] Unfortunately, we could not find the force fields and parametrizations for NaSCN and KSCN molten salts which precluded modeling of that solvent system. We studied a system consisting of bulk $BMIM^+Cl^-$ as well as systems including NCs (see Methods for model details). Figure 5c shows the simulated PDF of the bulk $BMIM^+Cl^-$ which is well matched to the experimental data obtained from the total X-ray scattering from pure $BMIM^+Cl^-$. The computed partial PDFs suggest that the intermolecular intermediate range order is dominated by $BMIM^+-Cl^-$ correlations (orange curve). We also extracted the density profiles of $BMIM^+Cl^-$ normal to the In-terminated (001) surface of a cubic zinc-blende InP NC. We plot these profiles, which vary with distance (z) from the NC surface along with

DOI: 10.1021/acsnano.9b01292
ACS Nano XXXX, XXX, XXX−XXX

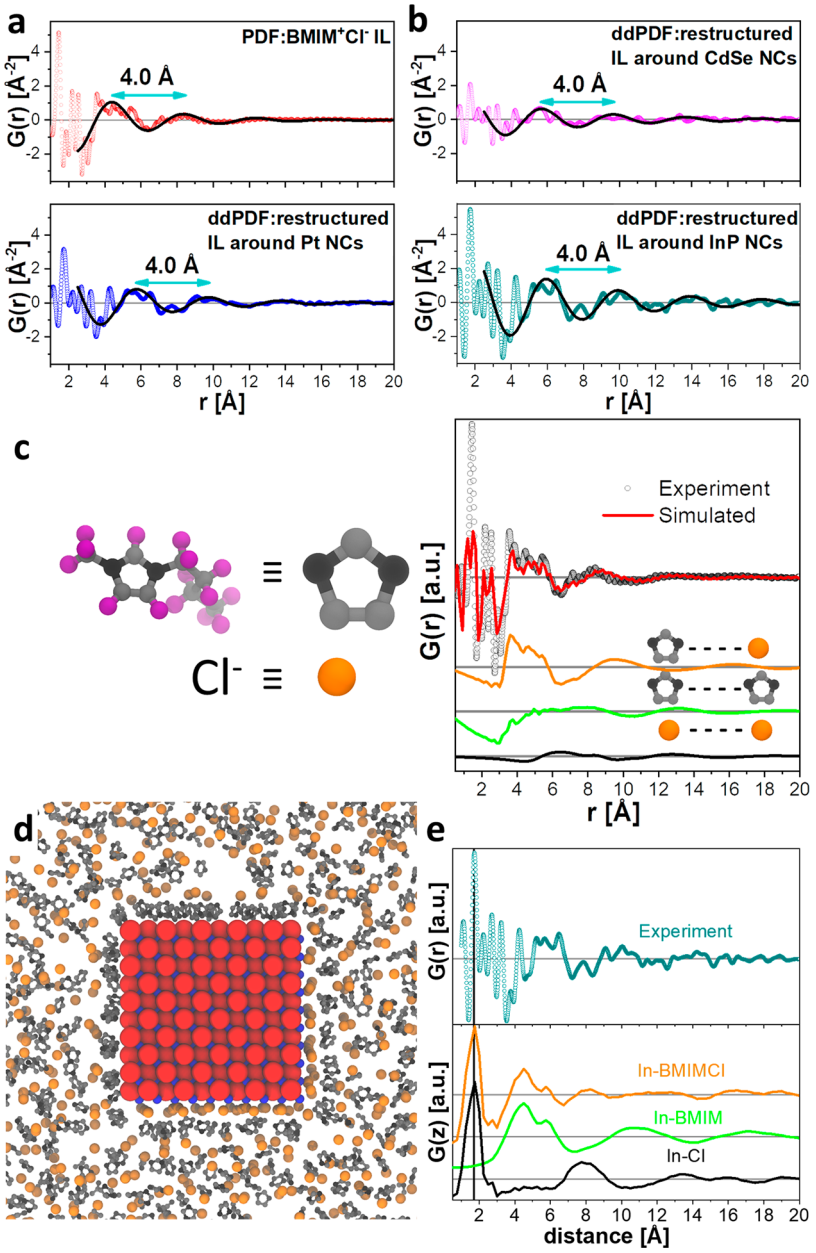

Figure 5. (a, b) Comparison of the dd-PDFs corresponding to the restructured $BMIM^+Cl^-$ melt around Pt, CdSe and InP NCs with PDF of bulk $BMIM^+Cl^-$ IL (black curves represent the fits). (c) Comparison of the experimental PDF with the simulated radial PDF of the bulk $BMIM^+Cl^-$ IL, and contributions from the inter-ion structures of $BMIM^+-Cl^-$, $BMIM^+-BMIM^+$, and Cl^--Cl^-. (d) MD snapshot (zoomed in view) of $BMIM^+Cl^-$ in the vicinity of the cubic zinc blende InP NC (In atoms are blue circles; P atoms are red circles). (e) Comparison of the experimental PDF with the simulated linear PDF in the direction normal to In-rich NC surface, and contributions from the surface-ion correlations of In-$BMIM^+$, In$-Cl^-$.

experimental dd-PDF, which varies with the radial distance (r) (Figure 5e). Interestingly, these measurements show a good match, in particular, between the small-distance large peak (at 1.7 Å), identified from the simulations as the Cl^- ion adhered to the In surface, and the second broad peak (~4–6 Å), identified as a layer of $BMIM^+$ ions immediately following the first Cl^- layer. A snapshot of the simulation (Figure 5d) clearly suggests that Cl^- ions form a dense layer on the In-terminated surface followed by a dense layer of $BMIM^+$ ions before the density correlations become bulk-like. Recent elemental analysis of InP NCs with Rutherford backscattering spectroscopy and XPS suggests that InP NCs are almost 100% In terminated.[52] Hence, there should be little contribution from the correlations between negatively charged (P terminated) facets and $BMIM^+$ ions to the total pair distribution function (Figure S20). The features of this surface-induced density profile do not change significantly for the different surfaces presented by InP and CdSe NCs in simulation (Figure S21), nor for the Pt NCs in experiment (Figure 5a). Thus, the restructuring of the $BMIM^+Cl^-$ solvent by a metal rich surface is robust to changes in the specific composition of the surface. Further, the restructuring observed in the experiment appears to consist largely of the order induced normal (z) to the NC surface.

In a control experiment, we dispersed organic ligand free CdSe NCs in the Lewis neutral $BMIM^+BF_4^-$ IL and performed

DOI: 10.1021/acsnano.9b01292
ACS Nano XXXX, XXX, XXX−XXX

analogous PDF analysis. The RSF obtained after bulk IL background subtraction contained the diffraction peaks of CdSe phase only, and there were no signs of the restructured solvent FSDP (Figure S22). Together with the SAXS results presented in Figure 2c for CdSe dispersed in $BMIM^+BF_4^-$, it is evident that solvent restructuring around the NC surface correlates with the observation of colloidal stability of NCs in highly ionic media. The universal restructuring observed in the Lewis basic NaSCN/KSCN melt and $BMIM^+Cl^-$ IL around various classes of NCs and its absence in the Lewis neutral $BMIM^+BF_4^-$ IL support the hypothesis of Zhang et al.[11] that the intermediate-range ionic ordering near the NC interface is responsible for the colloidal stability. SCN^- and Cl^- ions are able to act as X-type ligands which bind to electron deficient metal rich facets of NCs (Figure 3) and hence form a dense surface-bound layer (Figure 5d). BF_4^- ions, on the other hand, cannot act as X-type ligands and hence do not form a surface-bound layer. A layer of negatively charged surface-bound Cl^- in the case of $BMIM^+Cl^-$ IL and SCN^- in the case of NaSCN/KSCN molten salt in-turn electrostatically templates a charge density wave consisting of layers of alternating ions with opposite charges (Figure 5e). Guided by local Coulomb forces, the charge density wave propagates into the solvent for a distance greatly exceeding the Debye screening length, which is limited to one ion layer. These long-range ionic correlations in molten salts are not predicted by the Debye–Hückel theory and require accounting for both long-range Coulomb and short-range molecular interactions.[29] The charge density wave represented by the typical dd-PDF of 4.0 nm Pt NCs in NaSCN/KSCN melt (Figure 4b) decays to the bulk melt density at the distance of more than 20 Å away from the Pt surface. The associated oscillatory potential is only weakly perturbed by the van der Waals attraction in the interparticle distance range of 1 Å to 20 Å (Figure 6). As a result, the charge density wave generated by the NC surface can easily screen the van der Waals attraction and hence account for the colloidally stable dispersions in molten salts.

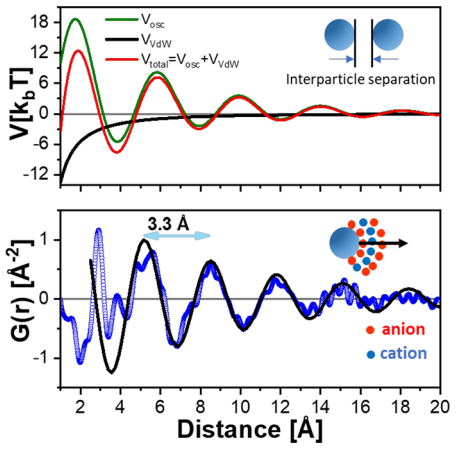

Figure 6. Comparison of the van der Waals and oscillatory potentials for Pt NCs (4.0 nm) interacting through NaSCN/KSCN melt with the experimental PDF of the restructured solvent around Pt NCs. "Distance" corresponds to the interparticle separation for the van der Waals and oscillatory potentials. The oscillatory potential is estimated using a modified phenomenological Ginsburg–Landau theory (see the Supporting Information for details on potential calculations).

CONCLUSIONS

In conclusion, X-ray PDF analysis and MD simulations provide evidence for the formation of a layered ionic solvation shell around NCs dispersed in molten inorganic salts and organic ionic liquids. The solvation shell has enhanced ion–ion correlations compared to the ions in the bulk liquid and extends far beyond the Debye screening length. The solvent restructuring happens only for those molten salts where ions are able to function as surface-bound ligands for dispersed NCs. Interestingly, ions in the NaSCN/KSCN melt exhibit more dramatic reorganization and increase in the correlation decay length near the NC surface than ions in the $BMIM^+Cl^-$ ionic liquid. SAXS analysis further corroborates that this solvation shell prevents direct approach of the NCs in various molten salts, hence rendering stable colloidal solutions. The charge density wave consisting of the restructured ions generates an oscillatory potential between NCs and hence constitutes a fundamentally different mechanism of colloidal stabilization in addition to the standard electrostatic and steric mechanisms. We believe that detailed understanding of the NC solvation in highly ionized media of inorganic melts and ionic liquids is necessary for the rational design of the colloidal systems in these unconventional media. The improved design of the colloidal state in the high temperature inorganic molten salts can assist development of a variety of hard-to-crystallize colloidal nanomaterials.

METHODS

Synthesis of NCs Capped with Organic Ligands. All NC syntheses were performed according to reported protocols using conventional air-free techniques including Schlenk line and N_2-filled glovebox. Pt NCs (mean size 4.0 ± 0.5 nm),[53] zinc-blende CdSe NCs (mean size 4.6 ± 0.5 nm),[54] ZrO_2 NCs (mean size 4.0 ± 0.4 nm),[55] InAs (mean size 5.0 ± 0.7 nm),[56] InP (mean size 4.7 nm ±0.6 nm),[57] and CdSe/CdS core–shell QDs (13.1 ± 1.3 nm)[58] were used in this work. Mean sizes were measured from SAXS analysis and verified with TEM measurements. All manipulations with molten salts and ILs were performed in a N_2-filled glovebox with moisture and oxygen levels under 0.1 ppm.

Pt NCs in $AlCl_3$/NaCl/KCl. Pt NCs were dispersed in a ternary mixture of $AlCl_3$/NaCl/KCl (63.5/20/16.5 mol %) through a direct phase transfer process. In this procedure, a solution of Pt NCs in anhydrous decane (capped with the original organic ligands, washed multiple times to remove excess organics) was interfaced with the molten salt mixture (4:1 vol ratio) in a glass vial. The resulting mixture was stirred at 120 °C using a Pyrex-glass-coated stir bar until NCs transferred completely from the upper decane phase to the molten salt phase. The upper phase was later discarded and fresh decane was added to the vial. This procedure was repeated several times to ensure complete removal of organic ligands.

CdSe/CdS and ZrO_2 NCs in NaSCN/KSCN. CdSe/CdS core–shell NCs were stripped of their organic ligands using tetrafluoroboric acid (HBF_4) as described in ref 59. ZrO_2 NCs were stripped of their organic ligands (tri-*n*-octyl phosphorus oxide) using nitrosonium tetrafluoroborate powder ($NOBF_4$).[60] Bare NCs form stable colloidal solutions in dimethylformamide and were precipitated with CH_3CN multiple times and dried as powders. A eutectic mixture of NaSCN/KSCN (26.3/73.7 mol %) was taken in a vial and heated to 250 °C until molten. The molten salt was cooled down to room temperature and ground into fine powder. Bare NC powder was then mixed with the finally ground eutectic mixture mixed and heated at 250 °C under stirring (using a Pyrex-glass-coated stir bar) for several hours until a stable solution was obtained.

Pt and InP NCs in NaSCN/KSCN. InP and Pt NCs were functionalized with S^{2-} using $(NH_4)_2S$ dissolved in formamide to form a stable colloidal solution.[61] These NCs were further transferred

DOI: 10.1021/acsnano.9b01292
ACS Nano XXXX, XXX, XXX–XXX

into toluene phase using didodecyldimethylammonium bromide (DDAB) as the phase transfer agent. This ligand decomposes cleanly into gaseous products via Hoffman elimination, leaving no organics behind.[62] The toluene phase containing NCs was transferred to a centrifuge tube, precipitated with ethanol to get rid of excess ligands, and redispersed in minimal amount of anhydrous toluene. The finally ground eutectic mixture of NaSCN/KSCN (see above) was combined with the solution of NCs capped with S^{2-}/DDA^{+} ion-pair in toluene and slowly heated at 250 °C under stirring (using the Pyrex-glass-coated stir bar) for several hours until a stable solution was obtained.

CdSe, InP, and InAs in $BMIM^{+}X^{-}$ ILs (X = Cl, Br, I, BF_4). NCs were dispersed in $BMIM^{+}X^{-}$ through a direct phase transfer process. In this procedure, a solution of NCs in anhydrous decane was combined with the respective IL (4:1 vol ratio) in a glass vial. Upon vigorous stirring at 100 °C (for $BMIM^{+}Cl^{-}$ and $BMIM^{+}Br^{-}$) and 50 °C ($BMIM^{+}I^{-}$), NCs gradually transferred into ILs within several hours, resulting in a colorless decane top phase. The bottom phase of the IL containing NCs was rinsed with fresh decane and ethyl acetate several times to get rid of the residual organic ligands. Afterward, a slightly turbid NC solution in IL was dissolved in CH_3CN and NCs were precipitated and supernatant discarded. The recovered NCs can be redispered in fresh halide containing $BMIM^{+}X^{-}$, forming a stable colloidal solution. Since BF_4^{-} anion is Lewis neutral and hence is not able to displace the original organic ligands, CdSe NCs were stripped off their organic ligands using $BMIM^{+}Cl^{-}$ IL as described above. The recovered CdSe NCs (after dissolution of $BMIM^{+}Cl^{-}$ matrix with CH_3CN) were further combined with $BMIM^{+}BF_4^{-}$ IL (liquid at room temperature). The resultant mixture failed to form a colloidally stable solution and remained turbid even after several hours of continuous stirring.

Characterization Techniques. The TEM images were obtained using 300 kV FEI Tecnai F30 microscope. FTIR spectra of Pt and CdSe/CdS NCs recovered from NaSCN/KSCN salt (by dissolving salt matrix in water) were acquired in the transmission mode using a NicoletNexus-670 FTIR spectrometer using KBr pellet as a substrate. XPS measurement was performed on a Kratos Axis Nova spectrometer using a monochromatic Al Kα source (1486.6 eV). ^{1}H NMR spectra were recorded at 500 MHz on a Bruker Ultrashield 500 plus spectrometer.

Small Angle X-ray Scattering (SAXS). Molten inorganic salt and IL samples were prepared by drawing the solution into 1.1 mm outer diameter (0.1 mm thickness) borosilicate glass capillaries and were further flame-sealed to avoid exposure to ambient atmosphere. The concentration for all the samples was ~1 mg/mL. All SAXS for the NC dispersions, except for CdSe/CdS core–shell NCs in NaSCN/KSCN molten salt, were collected at 12-ID-B at the Advanced Photon Source, Argonne National Laboratory, with the X-ray wavelength of 0.9341 Å. The *in situ* heating experiments were performed using Linkam stage. SAXS of CdSe/CdS core–shell NCs in NaSCN/KSCN molten salt were collected at 9-ID using an X-ray wavelength of 0.6902 Å. Please refer to the Supporting Information for details on SAXS modeling.

Total X-ray Scattering. Molten inorganic salt and IL samples were prepared by drawing the solution into 1.1 mm outer diameter (0.1 mm thickness) borosilicate glass capillaries and were further flame-sealed to avoid exposure to ambient atmosphere. High energy X-ray scattering data was collected at 11-ID-B at the Advanced Photon Source, Argonne National Laboratory, with the X-ray wavelength of 0.2113 Å. An *in situ* heating setup[63] was used to melt samples and collect X-ray data for various dispersions of NCs. KSCN/NaSCN samples were heated to 200 °C and $BMIM^{+}Cl^{-}$ IL samples were heated to 100 °C to ensure complete melting. The collected high energy X-ray scattering data was reduced to 1D in GSAS-II[64] using CeO_2 powder as a calibrant to determine sample to detector distance. Please refer to the Supporting Information for details on PDF extraction and analysis.

Molecular Dynamics Simulations. The $BMIM^{+}Cl^{-}$ IL system was studied using the CLDP force field for ionic liquids, a time step of 0.5 fs, and a short-ranged pairwise cutoff distance of 12 Å.[51] We ran molecular dynamics simulations using the LAMMPS software package[65] and visualized trajectories using the VMD package.[66] The long-range part of the Coulomb interaction was implemented using the particle–particle particle–mesh scheme, with relative error of 10^{-4}. Please refer to the Supporting Information for additional simulation details.

ASSOCIATED CONTENT

Supporting Information

The Supporting Information is available free of charge on the ACS Publications website at DOI: 10.1021/acsnano.9b01292.

Additional experimental details, extraction of PDF, fitting of PDF and SAXS curves, MD Simulation methods, Estimation of van der Waals and oscillatory potentials, TEM images, X-ray scattering data (PDF)

AUTHOR INFORMATION

Corresponding Author

*E-mail: dvtalapin@uchicago.edu.

ORCID

Nicholas B. Ludwig: 0000-0002-7345-659X
Hao Zhang: 0000-0003-4513-0813
Byeongdu Lee: 0000-0003-2514-8805
Karena W. Chapman: 0000-0002-8725-5633
Dmitri V. Talapin: 0000-0002-6414-8587

Present Address

[⊥]K.W.C.: Department of Chemistry, Stony Brook University, Stony Brook, New York 11790, United States.

Author Contributions

[‖]V.K., V.S., and N.B.L. contributed equally.

Notes

The authors declare no competing financial interest.

ACKNOWLEDGMENTS

We thank Dr. Kamila Wiaderek for helpful discussions regarding PDF analysis and Dr. Alexander Filatov for help with XPS measurements. We also thank Margaret Hudson for helpful discussions and critical review of the manuscript. This work was supported by the National Science Foundation under Award Number DMR-1611371, by the Office of Basic Energy Sciences, the US Department of Energy (Grant No. DE-SC0019375), by the Department of Defense (DOD) Air Force Office of Scientific Research under Grant Number FA9550-15-1-0099. V.S. was supported by the University of Chicago Materials Research Science and Engineering Center, which is funded by NSF under Award Number DMR-1420709. This research used resources of the Center for Nanoscale Materials and Advanced Photon Source, a U.S. Department of Energy (DOE) Office of Science User Facility operated for the DOE Office of Science by Argonne National Laboratory under Contract No. DE-AC02-06CH11357. We also acknowledge support from the University of Chicago Research Computing Center.

REFERENCES

(1) Murray, C. B.; Kagan, C. R.; Bawendi, M. G. Synthesis and Characterization of Monodisperse Nanocrystals and Close-Packed Nanocrystal Assemblies. *Annu. Rev. Mater. Sci.* **2000**, *30*, 545–610.
(2) Israelachvili, J. N. *Intermolecular and Surface Forces*; Academic Press: London, 2011.
(3) Boles, M. A.; Ling, D.; Hyeon, T.; Talapin, D. V. The Surface Science of Nanocrystals. *Nat. Mater.* **2016**, *15*, 141.

DOI: 10.1021/acsnano.9b01292
ACS Nano XXXX, XXX, XXX–XXX

(4) Talapin, D. V.; Rogach, A. L.; Kornowski, A.; Haase, M.; Weller, H. Highly Luminescent Monodisperse CdSe and CdSe/ZnS Nanocrystals Synthesized in a Hexadecylamine−Trioctylphosphine Oxide−Trioctylphospine Mixture. *Nano Lett.* **2001**, *1*, 207−211.
(5) Mourdikoudis, S.; Liz-Marzán, L. M. Oleylamine in Nanoparticle Synthesis. *Chem. Mater.* **2013**, *25*, 1465−1476.
(6) Murray, C. B.; Norris, D. J.; Bawendi, M. G. Synthesis and Characterization of Nearly Monodisperse CdE (E = Sulfur, Selenium, Tellurium) Semiconductor Nanocrystallites. *J. Am. Chem. Soc.* **1993**, *115*, 8706−8715.
(7) Park, J.; An, K.; Hwang, Y.; Park, J.-G.; Noh, H.-J.; Kim, J.-Y.; Park, J.-H.; Hwang, N.-M.; Hyeon, T. Ultra-Large-Scale Syntheses of Monodisperse Nanocrystals. *Nat. Mater.* **2004**, *3*, 891.
(8) Sun, S.; Murray, C. B.; Weller, D.; Folks, L.; Moser, A. Monodisperse FePt Nanoparticles and Ferromagnetic FePt Nanocrystal Superlattices. *Science* **2000**, *287*, 1989−1992.
(9) Srivastava, V.; Liu, W.; Janke, E. M.; Kamysbayev, V.; Filatov, A. S.; Sun, C.-J.; Lee, B.; Rajh, T.; Schaller, R. D.; Talapin, D. V. Understanding and Curing Structural Defects in Colloidal GaAs Nanocrystals. *Nano Lett.* **2017**, *17*, 2094−2101.
(10) Kanady, J. S.; Leidinger, P.; Haas, A.; Titlbach, S.; Schunk, S.; Schierle-Arndt, K.; Crumlin, E. J.; Wu, C. H.; Alivisatos, A. P. Synthesis of Pt_3Y and Other Early−Late Intermetallic Nanoparticles by Way of a Molten Reducing Agent. *J. Am. Chem. Soc.* **2017**, *139*, 5672−5675.
(11) Zhang, H.; Dasbiswas, K.; Ludwig, N. B.; Han, G.; Lee, B.; Vaikuntanathan, S.; Talapin, D. V. Stable Colloids in Molten Inorganic Salts. *Nature* **2017**, *542*, 328.
(12) Liu, X.; Fechler, N.; Antonietti, M. Salt Melt Synthesis of Ceramics, Semiconductors and Carbon Nanostructures. *Chem. Soc. Rev.* **2013**, *42*, 8237−8265.
(13) Sundermeyer, W. Fused Salts and Their Use as Reaction Media. *Angew. Chem., Int. Ed. Engl.* **1965**, *4*, 222−238.
(14) Volkov, S. V. Chemical Reactions in Molten Salts and Their Classification. *Chem. Soc. Rev.* **1990**, *19*, 21−28.
(15) Kerridge, D. H. Recent Advances in Molten Salts as Reaction Media. *Pure Appl. Chem.* **1975**, *41*, 355−371.
(16) Chen, G. Z.; Fray, D. J.; Farthing, T. W. Direct Electrochemical Reduction of Titanium Dioxide to Titanium in Molten Calcium Chloride. *Nature* **2000**, *407*, 361−364.
(17) Nohira, T.; Yasuda, K.; Ito, Y. Pinpoint and Bulk Electrochemical Reduction of Insulating Silicon Dioxide to Silicon. *Nat. Mater.* **2003**, *2*, 397−401.
(18) Cui, Z.; Chen, H.; Zhao, M.; Marshall, D.; Yu, Y.; Abruña, H.; DiSalvo, F. J. Synthesis of Structurally Ordered Pt_3Ti and Pt_3V Nanoparticles as Methanol Oxidation Catalysts. *J. Am. Chem. Soc.* **2014**, *136*, 10206−10209.
(19) Portehault, D.; Devi, S.; Beaunier, P.; Gervais, C.; Giordano, C.; Sanchez, C.; Antonietti, M. A General Solution Route toward Metal Boride Nanocrystals. *Angew. Chem., Int. Ed.* **2011**, *50*, 3262−3265.
(20) Liu, X.; Antonietti, M.; Giordano, C. Manipulation of Phase and Microstructure at Nanoscale for SiC in Molten Salt Synthesis. *Chem. Mater.* **2013**, *25*, 2021−2027.
(21) Liu, X.; Giordano, C.; Antonietti, M. A Molten-Salt Route for Synthesis of Si and Ge Nanoparticles: Chemical Reduction of Oxides by Electrons Solvated in Salt Melt. *J. Mater. Chem.* **2012**, *22*, 5454−5459.
(22) Shavel, A.; Guerrini, L.; Alvarez-Puebla, R. A. Colloidal Synthesis of Silicon Nanoparticles in Molten Salts. *Nanoscale* **2017**, *9*, 8157−8163.
(23) Liu, X.; Giordano, C.; Antonietti, M. A Facile Molten-Salt Route to Graphene Synthesis. *Small* **2014**, *10*, 193−200.
(24) Schwandt, C.; Dimitrov, A. T.; Fray, D. J. High-Yield Synthesis of Multi-Walled Carbon Nanotubes from Graphite by Molten Salt Electrolysis. *Carbon* **2012**, *50*, 1311−1315.
(25) Srivastava, V.; Kamysbayev, V.; Hong, L.; Dunietz, E.; Klie, R. F.; Talapin, D. V. Colloidal Chemistry in Molten Salts: Synthesis of Luminescent $In_{1-x}Ga_xP$ and $In_{1-x}Ga_xAs$ Quantum Dots. *J. Am. Chem. Soc.* **2018**, *140*, 12144−12151.
(26) Gebbie, M. A.; Dobbs, H. A.; Valtiner, M.; Israelachvili, J. N. Long-Range Electrostatic Screening in Ionic Liquids. *Proc. Natl. Acad. Sci. U. S. A.* **2015**, *112*, 7432−7437.
(27) Smith, A. M.; Lee, A. A.; Perkin, S. The Electrostatic Screening Length in Concentrated Electrolytes Increases with Concentration. *J. Phys. Chem. Lett.* **2016**, *7*, 2157−2163.
(28) Lee, A. A.; Perez-Martinez, C. S.; Smith, A. M.; Perkin, S. Scaling Analysis of the Screening Length in Concentrated Electrolytes. *Phys. Rev. Lett.* **2017**, *119*, No. 026002.
(29) Ludwig, N. B.; Dasbiswas, K.; Talapin, D. V.; Vaikuntanathan, S. Describing Screening in Dense Ionic Fluids with a Charge-Frustrated Ising Model. *J. Chem. Phys.* **2018**, *149*, 164505.
(30) Gebbie, M. A.; Smith, A. M.; Dobbs, H. A.; Lee, A. A.; Warr, G. G.; Banquy, X.; Valtiner, M.; Rutland, M. W.; Israelachvili, J. N.; Perkin, S.; Atkin, R. Long Range Electrostatic Forces in Ionic Liquids. *Chem. Commun.* **2017**, *53*, 1214−1224.
(31) Mezger, M.; Schröder, H.; Reichert, H.; Schramm, S.; Okasinski, J. S.; Schöder, S.; Honkimäki, V.; Deutsch, M.; Ocko, B. M.; Ralston, J.; Rohwerder, M.; Stratmann, M.; Dosch, H. Molecular Layering of Fluorinated Ionic Liquids at a Charged Sapphire (0001) Surface. *Science* **2008**, *322*, 424−428.
(32) Cremer, T.; Stark, M.; Deyko, A.; Steinrück, H. P.; Maier, F. Liquid/Solid Interface of Ultrathin Ionic Liquid Films: $[C_1C_1Im]$-$[Tf_2N]$ and $[C_8C_1Im][Tf_2N]$ on Au(111). *Langmuir* **2011**, *27*, 3662−3671.
(33) Jeon, Y.; Sung, J.; Bu, W.; Vaknin, D.; Ouchi, Y.; Kim, D. Interfacial Restructuring of Ionic Liquids Determined by Sum-Frequency Generation Spectroscopy and X-Ray Reflectivity. *J. Phys. Chem. C* **2008**, *112*, 19649−19654.
(34) Zobel, M.; Neder, R. B.; Kimber, S. A. J. Universal Solvent Restructuring Induced by Colloidal Nanoparticles. *Science* **2015**, *347*, 292−294.
(35) Thomä, S. L. J.; Krauss, S. W.; Eckardt, M.; Chater, P.; Zobel, M. Atomic Insight into Hydration Shells around Facetted Nanoparticles. *Nat. Commun.* **2019**, *10*, 995.
(36) Futamura, R.; Iiyama, T.; Takasaki, Y.; Gogotsi, Y.; Biggs, M. J.; Salanne, M.; Ségalini, J.; Simon, P.; Kaneko, K. Partial Breaking of the Coulombic Ordering of Ionic Liquids Confined in Carbon Nanopores. *Nat. Mater.* **2017**, *16*, 1225.
(37) Zhang, H.; Jang, J.; Liu, W.; Talapin, D. V. Colloidal Nanocrystals with Inorganic Halide, Pseudohalide, and Halometallate Ligands. *ACS Nano* **2014**, *8*, 7359−7369.
(38) Dirin, D. N.; Dreyfuss, S.; Bodnarchuk, M. I.; Nedelcu, G.; Papagiorgis, P.; Itskos, G.; Kovalenko, M. V. Lead Halide Perovskites and Other Metal Halide Complexes as Inorganic Capping Ligands for Colloidal Nanocrystals. *J. Am. Chem. Soc.* **2014**, *136*, 6550−6553.
(39) Fafarman, A. T.; Koh, W.-k.; Diroll, B. T.; Kim, D. K.; Ko, D.-K.; Oh, S. J.; Ye, X.; Doan-Nguyen, V.; Crump, M. R.; Reifsnyder, D. C.; Murray, C. B.; Kagan, C. R. Thiocyanate-Capped Nanocrystal Colloids: Vibrational Reporter of Surface Chemistry and Solution-Based Route to Enhanced Coupling in Nanocrystal Solids. *J. Am. Chem. Soc.* **2011**, *133*, 15753−15761.
(40) Li, T.; Senesi, A. J.; Lee, B. Small Angle X-Ray Scattering for Nanoparticle Research. *Chem. Rev.* **2016**, *116*, 11128−11180.
(41) Beaucage, G. Small-Angle Scattering from Polymeric Mass Fractals of Arbitrary Mass-Fractal Dimension. *J. Appl. Crystallogr.* **1996**, *29*, 134−146.
(42) Sorensen, C. M. Light Scattering by Fractal Aggregates: A Review. *Aerosol Sci. Technol.* **2001**, *35*, 648−687.
(43) Liu, Y.; Han, X.; He, L.; Yin, Y. Thermoresponsive Assembly of Charged Gold Nanoparticles and Their Reversible Tuning of Plasmon Coupling. *Angew. Chem., Int. Ed.* **2012**, *51*, 6373−6377.
(44) Zhang, H.; Wang, D. Controlling the Growth of Charged-Nanoparticle Chains through Interparticle Electrostatic Repulsion. *Angew. Chem., Int. Ed.* **2008**, *47*, 3984−3987.
(45) Lee, B.; Podsiadlo, P.; Rupich, S.; Talapin, D. V.; Rajh, T.; Shevchenko, E. V. Comparison of Structural Behavior of Nanocrystals in Randomly Packed Films and Long-Range Ordered Superlattices by

DOI: 10.1021/acsnano.9b01292
ACS Nano XXXX, XXX, XXX−XXX

Time-Resolved Small Angle X-Ray Scattering. *J. Am. Chem. Soc.* **2009**, *131*, 16386−16388.
(46) Johnson, K.; Inman, D.; Saboungi, M.; Newman, D. *Proceedings of the Fifth International Symposium on Molten Salts*; The Electrochemical Society: Pennington, NJ, 1985.
(47) Freeland, B. H.; Habeeb, J. J.; Tuck, D. G. Coordination Compounds of Indium. Part XXXIII. X-Ray Photoelectron Spectroscopy of Neutral and Anionic Indium Halide Species. *Can. J. Chem.* **1977**, *55*, 1527−1532.
(48) Donley, C.; Dunphy, D.; Paine, D.; Carter, C.; Nebesny, K.; Lee, P.; Alloway, D.; Armstrong, N. R. Characterization of Indium−Tin Oxide Interfaces Using X-Ray Photoelectron Spectroscopy and Redox Processes of a Chemisorbed Probe Molecule: Effect of Surface Pretreatment Conditions. *Langmuir* **2002**, *18*, 450−457.
(49) Fannin, A. A.; King, L. A.; Seegmiller, D. W. Chloroaluminate Equilibria in $AlCl_3$ - NaCl Melts. *J. Electrochem. Soc.* **1972**, *119*, 801−807.
(50) Leote de Carvalho, R. J. F.; Evans, R. The Decay of Correlations in Ionic Fluids. *Mol. Phys.* **1994**, *83*, 619−654.
(51) Canongia Lopes, J. N.; Deschamps, J.; Pádua, A. A. H. Modeling Ionic Liquids Using a Systematic All-Atom Force Field. *J. Phys. Chem. B* **2004**, *108*, 2038−2047.
(52) Kim, T.-G.; Zherebetskyy, D.; Bekenstein, Y.; Oh, M. H.; Wang, L.-W.; Jang, E.; Alivisatos, A. P. Trap Passivation in Indium-Based Quantum Dots through Surface Fluorination: Mechanism and Applications. *ACS Nano* **2018**, *12*, 11529−11540.
(53) Wang, C.; Daimon, H.; Onodera, T.; Koda, T.; Sun, S. A General Approach to the Size- and Shape-Controlled Synthesis of Platinum Nanoparticles and Their Catalytic Reduction of Oxygen. *Angew. Chem., Int. Ed.* **2008**, *47*, 3588−3591.
(54) Mohamed, M. B.; Tonti, D.; Al-Salman, A.; Chemseddine, A.; Chergui, M. Synthesis of High Quality Zinc Blende CdSe Nanocrystals. *J. Phys. Chem. B* **2005**, *109*, 10533−10537.
(55) Joo, J.; Yu, T.; Kim, Y. W.; Park, H. M.; Wu, F.; Zhang, J. Z.; Hyeon, T. Multigram Scale Synthesis and Characterization of Monodisperse Tetragonal Zirconia Nanocrystals. *J. Am. Chem. Soc.* **2003**, *125*, 6553−6557.
(56) Guzelian, A. A.; Banin, U.; Kadavanich, A. V.; Peng, X.; Alivisatos, A. P. Colloidal Chemical Synthesis and Characterization of InAs Nanocrystal Quantum Dots. *Appl. Phys. Lett.* **1996**, *69*, 1432−1434.
(57) Xie, R.; Battaglia, D.; Peng, X. Colloidal InP Nanocrystals as Efficient Emitters Covering Blue to Near-Infrared. *J. Am. Chem. Soc.* **2007**, *129*, 15432−15433.
(58) Chen, O.; Zhao, J.; Chauhan, V. P.; Cui, J.; Wong, C.; Harris, D. K.; Wei, H.; Han, H.-S.; Fukumura, D.; Jain, R. K.; Bawendi, M. G. Compact High-Quality CdSe−CdS Core−Shell Nanocrystals with Narrow Emission Linewidths and suppressed Blinking. *Nat. Mater.* **2013**, *12*, 445.
(59) Huang, J.; Liu, W.; Dolzhnikov, D. S.; Protesescu, L.; Kovalenko, M. V.; Koo, B.; Chattopadhyay, S.; Shenchenko, E. V.; Talapin, D. V. Surface Functionalization of Semiconductor and Oxide Nanocrystals with Small Inorganic Oxoanions (PO_4^{3-}, MoO_4^{2-}) and Polyoxometalate Ligands. *ACS Nano* **2014**, *8*, 9388−9402.
(60) Dong, A.; Ye, X.; Chen, J.; Kang, Y.; Gordon, T.; Kikkawa, J. M.; Murray, C. B. A Generalized Ligand-Exchange Strategy Enabling Sequential Surface Functionalization of Colloidal Nanocrystals. *J. Am. Chem. Soc.* **2011**, *133*, 998−1006.
(61) Nag, A.; Kovalenko, M. V.; Lee, J.-S.; Liu, W.; Spokoyny, B.; Talapin, D. V. Metal-Free Inorganic Ligands for Colloidal Nanocrystals: S^{2-}, HS^-, Se^{2-}, HSe^-, Te^{2-}, HTe^-, TeS_3^{2-}, OH^-, and NH_2^- as Surface Ligands. *J. Am. Chem. Soc.* **2011**, *133*, 10612−10620.
(62) Kovalenko, M. V.; Bodnarchuk, M. I.; Talapin, D. V. Nanocrystal Superlattices with Thermally Degradable Hybrid Inorganic−Organic Capping Ligands. *J. Am. Chem. Soc.* **2010**, *132*, 15124−15126.
(63) Chupas, P. J.; Chapman, K. W.; Kurtz, C.; Hanson, J. C.; Lee, P. L.; Grey, C. P. A Versatile Sample-Environment Cell for Non-Ambient X-Ray Scattering Experiments. *J. Appl. Crystallogr.* **2008**, *41*, 822−824.
(64) Toby, B. H.; Von Dreele, R. B. Gsas-Ii: The Genesis of a Modern Open-Source All Purpose Crystallography Software Package. *J. Appl. Crystallogr.* **2013**, *46*, 544−549.
(65) Plimpton, S. Fast Parallel Algorithms for Short-Range Molecular Dynamics. *J. Comput. Phys.* **1995**, *117*, 1−19.
(66) Humphrey, W.; Dalke, A.; Schulten, K. Vmd: Visual Molecular Dynamics. *J. Mol. Graphics* **1996**, *14*, 33−38.

DOI: 10.1021/acsnano.9b01292
ACS Nano XXXX, XXX, XXX−XXX